

distribution function is updated with allowance for nucleation of new particles and growth/dissolution of the preexisting ones.

At step k with nucleation rate $J_c^{(k)}$ according to Eq. (1), the number of freshly formed particles is $J_c^{(k)}\delta t^{(k)}$. These particles form a new class with a characteristic size $R_c^{(k)} = (1 + \alpha_{R_c})R_c$, slightly exceeding the critical one ($\alpha_{R_c} \ll 1$ is the fitting parameter), to enable their growth during the next step. Besides, the size change due to the growth/dissolution is checked for the previously nucleated particles. To this end, Eq. (10) is applied. To admit the complete dissolution, the minimal radius R_{min} of the persisting particles is introduced. We will use $R_{min} = R_c(T = 20^\circ\text{C})$, where $R_c(T = 20^\circ\text{C})$ is the critical embryo size at room temperature. The proposed algorithm enables the satisfactorily accurate integration of the simultaneous differential equations describing concurrent phenomena of the particles nucleation, growth, and coalescence.

To treat the precipitation phenomena at non-isothermal conditions, additive pseudo-isothermal contributions are considered. The temperature of any step in this approximation is selected according to the given heating/cooling rate whereas all temperature-dependent parameters are updated at each next step.

The performance of this algorithm significantly depends on the time step. To ensure accuracy and convergence of computations, this step should be appropriately short. We make use of the three constraints as follows.

First,

$$\delta t^{(k)} < \delta t_1 = \frac{0.01 X_{AE}^{(k)}}{|X_{AE}^{(k)} - X_{AE}^{(k-1)}|} \delta t^{(k-1)}, \quad (14)$$

ensures negligible variations (less than 0.01) of alloying amounts in the solid solution relative to the current level. The second condition

$$\delta t^{(k)} < \delta t_2 = \frac{0.01 V_p^{(k)}}{|V_p^{(k)} - V_p^{(k-1)}|} \delta t^{(k-1)}, \quad (15)$$

limits the relative change of particles volume to 0.01. The third constraint is imposed on the precipitation under non-isothermal conditions:

$$\delta t^{(k)} < \delta t_3 = \frac{\Delta T^{(k)}}{V_T}, \quad (16)$$

where $\Delta T^{(k)}$ is the temperature change during step k , V_T is the magnitude of the average cooling/heating rate. This condition limits the temperature variation that should not exceed one degree per one step i.e. maximum $\delta t_3 = V_T^{-1}$. Allowing for all three constraints, we select $\delta t^{(k)} = \min\{\delta t_1; \delta t_2; \delta t_3\}$.

4. Equilibrium concentrations of dissolved alloying elements in α -phase and thermodynamic driving forces in the nucleation of dispersed particles

Thermodynamic driving forces for precipitation of SAE carbides are derived from the temperature-dependent products of their and carbon solubility [21]. The formation of any carbide may be described by equation $xMe + yC = Me_xC_y$. To evaluate the related driving force, we use the expression

$$\Delta G_V^{Me_xC_y} = -\frac{R_g T}{V_m^{Me_xC_y}} \left(x \ln \frac{X_{Me}}{X_{Me}^{eq}} + y \ln \frac{X_C}{X_C^{eq}} \right), \quad (17)$$

where $V_m^{Me_xC_y} = V_{FU}^{Me_xC_y} N_A$ is the molar volume of Me_xC_y , $V_{FU}^{Me_xC_y}$ is the corresponding FU volume, N_A is the Avogadro number. According to Eq. (17), driving forces to form the considered carbides are:

$$\text{Fe}_3\text{C}: \Delta G_V^{Fe_3C} = -\frac{R_g T}{V_m^{Fe_3C}} \left(3 \ln \frac{1 - X_C}{1 - X_C^{eq}} + \ln \frac{X_C}{X_C^{eq}} \right), \quad (18)$$

$$\text{V}_4\text{C}_3: \Delta G_V^{V_4C_3} = -\frac{R_g T}{V_m^{V_4C_3}} \left(4 \ln \frac{X_V}{X_V^{eq}} + 3 \ln \frac{X_C}{X_C^{eq}} \right), \quad (19)$$

$$\text{Mo}_2\text{C}: \Delta G_V^{Mo_2C} = -\frac{R_g T}{V_m^{Mo_2C}} \left(2 \ln \frac{X_{Mo}}{X_{Mo}^{eq}} + \ln \frac{X_C}{X_C^{eq}} \right), \quad (20)$$

$$\text{Cr}_7\text{C}_3: \Delta G_V^{Cr_7C_3} = -\frac{R_g T}{V_m^{Cr_7C_3}} \left(7 \ln \frac{X_{Cr}}{X_{Cr}^{eq}} + 3 \ln \frac{X_C}{X_C^{eq}} \right). \quad (21)$$

Following [22], the equilibrium molar fraction of the dissolved carbon in α -phase takes on the form

$$X_C^{eq} = 0.01 \times \exp \left(-\frac{28400}{R_g T} \right). \quad (22)$$

To evaluate equilibrium amounts of V, Mo, and Cr, simultaneous equations for solubility products and the mass balance should be solved [21]. In the simple case of only one element (for example, V) these equations are reduced to

$$X_V^{eq} X_C^{eq} = K_{V_4C_3} \quad (23)$$

$$\frac{3}{4} (X_V^0 - X_V^{eq}) = X_C^0 - X_C^{eq},$$

where $K_{V_4C_3}$ is the solubility product for carbide V_4C_3 . At high temperatures where $X_V^0 X_C^0 \leq K_{V_4C_3}$ (no particles), system (23) leads to $X_V^{eq} = X_V^0$, whereas at lower temperatures ($X_V^0 X_C^0 > K_{V_4C_3}$)

$$X_C^{eq} = \frac{1}{2} \left[-\left(\frac{3}{4} X_V^0 - X_C^0 \right) + \sqrt{\left(\frac{3}{4} X_V^0 - X_C^0 \right)^2 + 3K_{V_4C_3}} \right], \quad (24)$$

$$X_V^{eq} = \frac{K_{V_4C_3}}{X_C^{eq}}.$$

In a more complicated case of two SAE involved, e.g. V and Mo, the system of the equation takes on the form

$$X_V^{eq} X_C^{eq} = K_{V_4C_3},$$

$$X_{Mo}^{eq} X_C^{eq} = K_{Mo_2C}, \quad (25)$$

$$\frac{3}{4} (X_V^0 - X_V^{eq}) + \frac{1}{2} (X_{Mo}^0 - X_{Mo}^{eq}) = X_C^0 - X_C^{eq}.$$

Accordingly, at high temperature ($X_V^0 X_C^0 \leq K_{V_4C_3}$ and $X_{Mo}^0 X_C^0 \leq K_{Mo_2C}$) there is no precipitation and $X_V^{eq} = X_V^0$, $X_{Mo}^{eq} = X_{Mo}^0$, while whether $X_V^0 X_C^0 > K_{V_4C_3}$ or $X_{Mo}^0 X_C^0 > K_{Mo_2C}$ at lower temperature leads to

$$X_C^{eq} = \frac{1}{2} \left[-\left(\frac{3}{4} X_V^0 - X_C^0\right) + \sqrt{\left(\frac{3}{4} X_V^0 - X_C^0\right)^2 + 3K_{V_4C_3}} \right],$$

$$X_V^{eq} = \frac{K_{V_4C_3}}{X_C^{eq}},$$

$$X_{Mo}^{eq} = X_{Mo}^0.$$

If $X_V^0 X_C^0 > K_{V_4C_3}$ and $X_{Mo}^0 X_C^0 \leq K_{Mo_2C}$, as well as at $X_V^0 X_C^0 \leq K_{V_4C_3}$ and $X_{Mo}^0 X_C^0 > K_{Mo_2C}$,

$$X_C^{eq} = \frac{1}{2} \left[-\left(\frac{1}{2} X_{Mo}^0 - X_C^0\right) + \sqrt{\left(\frac{1}{2} X_{Mo}^0 - X_C^0\right)^2 + 2K_{Mo_2C}} \right],$$

$$X_{Mo}^{eq} = \frac{K_{Mo_2C}}{X_C^{eq}},$$

$$X_V^{eq} = X_V^0.$$

When the temperature is further reduced so that $X_V^0 X_C^0 > K_{V_4C_3}$, $X_{Mo}^0 X_C^0 > K_{Mo_2C}$, and $X_V^0 X_C^0 / K_{V_4C_3}$ approaches $X_{Mo}^0 X_C^0 / K_{Mo_2C}$, the analysis is made as follows. The equilibrium molar fraction of carbon at $X_V^0 X_C^0 / K_{V_4C_3} > X_{Mo}^0 X_C^0 / K_{Mo_2C}$, is expressed by Eq. (25) and additional condition

$$X_{Mo}^0 X_C^{eq} > K_{Mo_2C},$$

is checked. If the latter is the case, both considered carbides coexist. Otherwise, only V_4C_3 is admitted. In case of $X_{Mo}^0 X_C^0 / K_{Mo_2C} > X_V^0 X_C^0 / K_{V_4C_3}$, the carbon amount is expressed by Eq. (27) and another condition

$$X_V^0 X_C^{eq} > K_{V_4C_3},$$

is checked. When the latter is satisfied, the two carbides may coexist; otherwise, only Mo_2C is admitted. In case of the coexistence

$$X_C^{eq} = \frac{1}{2} \left[-\left(\frac{3}{4} X_V^0 + \frac{1}{2} X_{Mo}^0 - X_C^0\right) + \sqrt{\left(\frac{3}{4} X_V^0 + \frac{1}{2} X_{Mo}^0 - X_C^0\right)^2 + 4\left(\frac{3}{4} K_{V_4C_3} + \frac{1}{2} K_{Mo_2C}\right)} \right],$$

$$X_V^{eq} = \frac{K_{V_4C_3}}{X_C^{eq}},$$

$$X_{Mo}^{eq} = \frac{K_{Mo_2C}}{X_C^{eq}}.$$

In the case of the reaction involving three elements the simultaneous equations

$$X_V^{eq} X_C^{eq} = K_{V_4C_3},$$

$$X_{Mo}^{eq} X_C^{eq} = K_{Mo_2C},$$

$$X_{Cr}^{eq} X_C^{eq} = K_{Cr_7C_3},$$

$$\frac{3}{4}(X_V^0 - X_V^{eq}) + \frac{1}{2}(X_{Mo}^0 - X_{Mo}^{eq}) + \frac{3}{7}(X_{Cr}^0 - X_{Cr}^{eq}) = X_C^0 - X_C^{eq},$$

should be treated. Volume fractions of the carbides are then derived from equilibrium concentrations:

$$\begin{aligned}
 f_{V_4C_3} &= \frac{X_V^0 - X_V^{eq}}{X_V^{V_4C_3} - X_V^{eq}}, \\
 f_{Mo_2C} &= \frac{X_{Mo}^0 - X_{Mo}^{eq}}{X_{Mo}^{Mo_2C} - X_{Mo}^{eq}}, \\
 f_{Cr_7C_3} &= \frac{X_{Cr}^0 - X_{Cr}^{eq}}{X_{Cr}^{Cr_7C_3} - X_{Cr}^{eq}}.
 \end{aligned} \tag{32}$$

To determine the corresponding solubility products, the following expressions are used:

$$\begin{aligned}
 K_{V_4C_3} &= \frac{M_{Fe}}{M_C M_V} 10^4 \cdot 10^{2.5 \frac{6000 - 5600[C]^{0.73} - 44.6[Mn] + 120[Si]}{T}}, \\
 K_{Mo_2C} &= \frac{M_{Fe}}{M_C M_{Mo}} 10^4 \cdot 10^{3.6 \frac{7500 - 3700[C]^{0.2} - 85[Mn] + 120[Si]}{T}}, \\
 K_{Cr_7C_3} &= \frac{M_{Fe}}{M_C M_{Cr}} 10^4 \cdot 10^{3.0 \frac{5700 - 4400[C]^{0.43}}{T}},
 \end{aligned} \tag{33}$$

where $M_{Fe}, M_C, M_V, M_{Mo}, M_{Cr}$ are atomic masses of related elements, [C], [Mn] and [Si] are corresponding concentrations (mass.%). Formulas (33) for solubility products of all considered carbides have been obtained with the Thermo-Calc software [23].

Table 1 represents the chemical compositions of 8 bainitic-martensitic steels. Respective calculations of temperature-dependent equilibrium volume fractions of carbides have been implemented according to both Thermo-Calc and the previously represented empirical expressions. As shown in Fig. 1, respective results do not significantly differ although our formulas are relatively simple and hence provide quick calculations.

Table 1. Chemical compositions (mass.%) of the investigated steels

Steel	C	Mn	Si	Cr	Ni	Cu	Mo	Nb	V	Ti
S1	0.21	0.56	0.25	0.75	0.10	0.14	0.02	0.002	0.003	0.002
S2	0.11	0.54	0.85	0.75	0.66	0.42	0.02	0.002	0.005	0.005
S3	0.10	1.57	0.27	0.02	0.01	0.02	-	0.036	0.039	0.014
S4	0.12	0.45	0.25	0.59	0.06	0.12	-	0.024	0.053	0.003
S5	0.10	1.56	0.29	0.12	0.13	0.13	0.01	0.044	0.066	0.005
S6	0.12	1.01	0.24	1.14	0.19	0.17	0.41	0.031	0.005	0.003
S7	0.27	0.58	1.09	0.85	1.42	0.06	0.23	0.023	0.007	0.045
S8	0.10	0.34	0.22	0.41	1.91	0.52	0.26	0.003	0.032	0.002

As to the thermodynamic driving force for the origination of Cu particles, this is expressed by

$$\Delta G_V^{Cu} = - \frac{R_g T}{V_m^{Cu}} \ln \frac{X_{Cu}}{X_{Cu}^{eq}}, \tag{34}$$

where V_m^{Cu} is the molar volume of Cu. Expressed in mass.%, its equilibrium amount w_{Cu}^{eq} at temperature T (°C) corresponds to

$$\ln \left[w_{Cu}^{eq} \right] = 7.35 - \frac{7574}{T}. \tag{35}$$

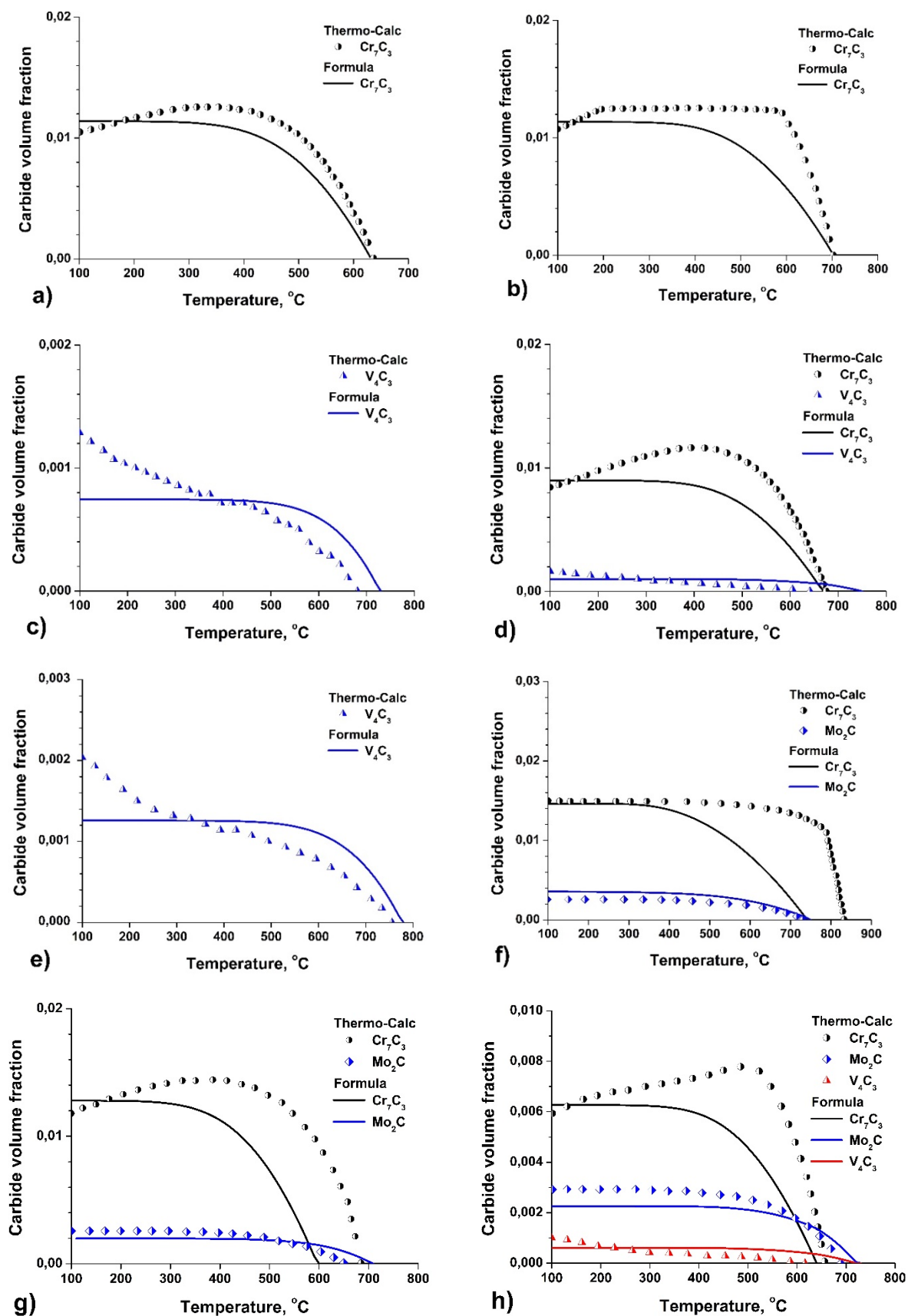


Fig. 1. Temperature dependences of equilibrium volume fractions calculated for the considered carbides by means of the present model and by Thermo-Calc. The results are shown for bainitic-martensitic steels: a) S1; b) S2; c) S3; d) S4; e) S5; f) S6; g) S7; h) S8

Constants in this formula have been derived by means of Thermo-Calc from a set of solvus temperatures T_S^{Cu} of Cu particles at various amounts of this element in alloy α -Fe-Cu. It follows from Eq. (35) that

$$T_S^{Cu} = \frac{7574}{7.35 - \ln[w_{Cu}]} \quad (36)$$

where the solvus temperature is expressed in K. As evident from Fig. 2, the latter expression provides quite satisfactory accuracy over a wide range of Cu amount dissolved in α -iron.

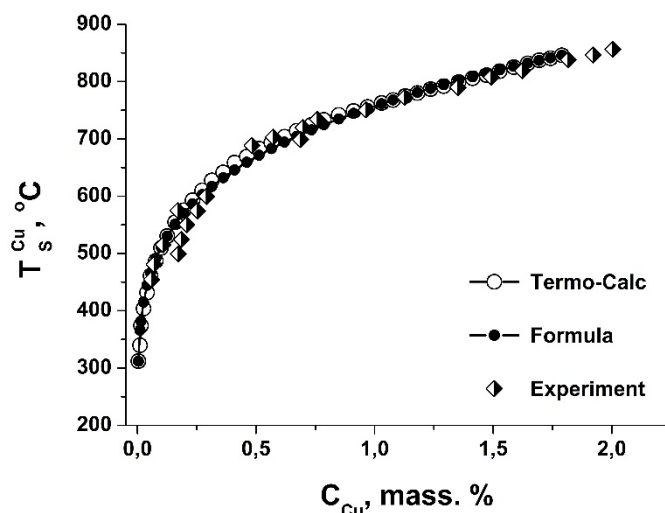


Fig. 2. Comparison of solvus temperature of Cu particles dependences on amount of this element in alloy α -Fe-Cu expressed by Eq. (36) and determined with Thermo-Calc with corresponding experimental data [12]

5. Comparison of modeling results to experimental data

When modeling precipitation of various particles, the diffusivity of involved elements has been treated as follows. To allow for the influence of main SAE (Mn, Ni, Cr, Mo, Si) on the carbon diffusion coefficient in the α -phase of steel, the authors' formula obtained in [24] is employed. Such coefficients for SAE themselves are expressed according to [3] and [25]:

$$D_V = 3.05 \times 10^{-4} \exp\left(-\frac{239000}{R_g T}\right) (m^2 s^{-1}), \quad (37)$$

$$D_{Mo} = 2.29 \times 10^{-4} \exp\left(-\frac{239000}{R_g T}\right) (m^2 s^{-1}), \quad (38)$$

$$D_{Cr} = 8.52 \times 10^{-4} \exp\left(-\frac{250400}{R_g T}\right) (m^2 s^{-1}). \quad (39)$$

As to Cu, its diffusion coefficients proposed in the literature suggest rather different activation energies (130 to 250 kJ/mol) [17,26-29]. As often remarked, evaluation of this coefficient for equilibrium conditions fails to describe the real precipitation kinetics of Cu in the quenched state or under irradiation [29]. Owing to significant oversaturation by vacancies in such non-equilibrium conditions, the effective activation energy proves to be much lesser. That is why, according to [17], the present model employs

$$D_{Cu} = 6 \times 10^{-8} \exp\left(-\frac{166400}{R_g T}\right) (m^2 s^{-1}). \tag{40}$$

Values of other parameters of our model are represented in Table 2. Note that values of $\gamma_{p/\alpha}$ (specific interfacial energies of particles in α -phase) have been determined in the model calibration as will be considered below.

Table 2. Model parameters for various particle types

	Parameter	Value $\times 10^{29}$
Volume per FU of phase particle, m^3	$V_{FU}^{Fe_3C}$	3.80
	$V_{FU}^{V_4C_3}$	7.41
	$V_{FU}^{Mo_2C}$	3.68
	$V_{FU}^{Cr_7C_3}$	7.91
	V_{FU}^{Cu}	1.18
Specific interfacial energies, J/m^2	$\gamma_{Fe_3C/\alpha}$	0.174
	$\gamma_{V_4C_3/\alpha}$	0.25
	$\gamma_{Mo_2C/\alpha}$	0.25
	$\gamma_{Cr_7C_3/\alpha}$	0.25
	$\gamma_{Cu/\alpha}$	0.35
Molar fractions of alloying elements in particles	$X_C^{Fe_3C}$	0.25
	$X_C^{V_4C_3}$	0.429
	$X_C^{Mo_2C}$	0.333
	$X_C^{Cr_7C_3}$	0.3
	$X_V^{V_4C_3}$	0.571
	$X_{Mo}^{Mo_2C}$	0.667
	$X_{Cr}^{Cr_7C_3}$	0.7
	X_{Cu}^{Cu}	1

Figures 3,4 provide a comparison of the predicted and experimental kinetics of Cu precipitation in alloy α -Fe+1.34Cu (mass.%) [9] that evidence for satisfactory performance of the model at practically important temperatures.

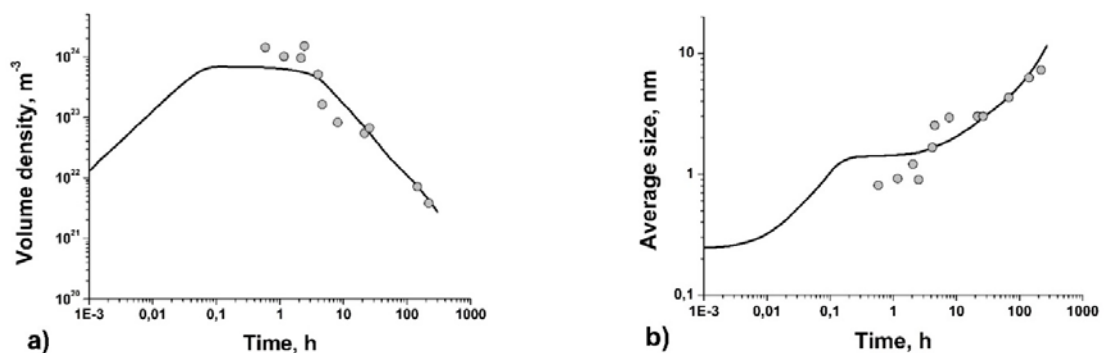


Fig. 3. Model (curves) and experimental (dots, [9]) time dependences of the volume fraction (a) and the average size (b) of Cu particles in aging of alloy α -Fe+1.34Cu (mass.%) at 500°C

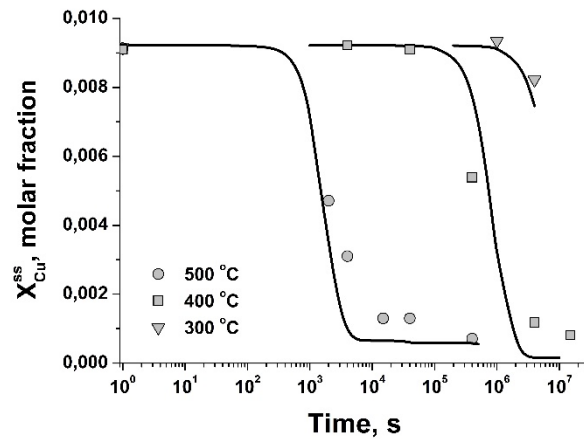


Fig. 4. Model (curves) and experimental (dots, [9]) time dependences of the Cu molar fraction in the solid solution in aging of alloy α -Fe+1.34Cu (mass.%) at various temperatures

Figures 5,6 represent results of the modeling of precipitation kinetics for V and Mo carbides during tempering of steels A and B [3] whose compositions are given in Table 3.

To sum up, the above-considered results support good correspondence of the present model with experimental data (volume fractions and average sizes) on Mo_2C and V_4C_3 precipitation when tempering investigated steels at the typical temperature of 600°C .

Table 3. Chemical composition (mass.%) of investigated steels

Steel	C	Si	Mn	Mo	V	Al	N
A	0.1	<0.005	1.99	1.6	-	0.03	0.0049
B	0.1	<0.005	1.95	-	0.57	0.03	0.0043

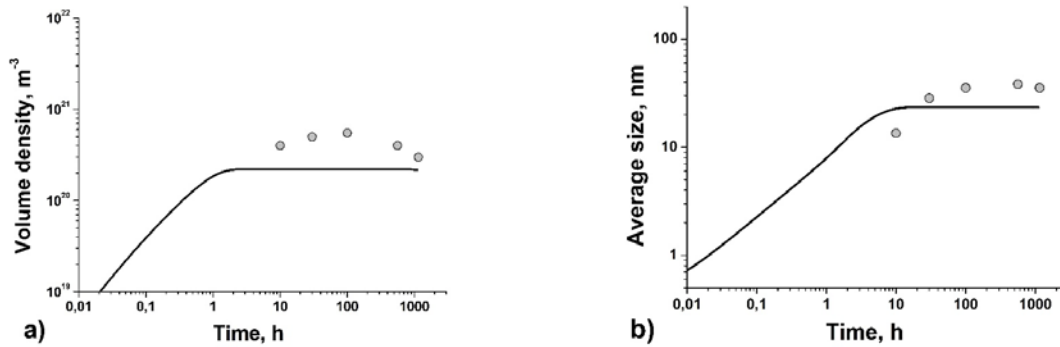


Fig. 5. Model (curves) and experimental (dots, [3]) time dependences of volume fraction (a) and the average size (b) of Mo_2C particles in tempering steel A at 600°C

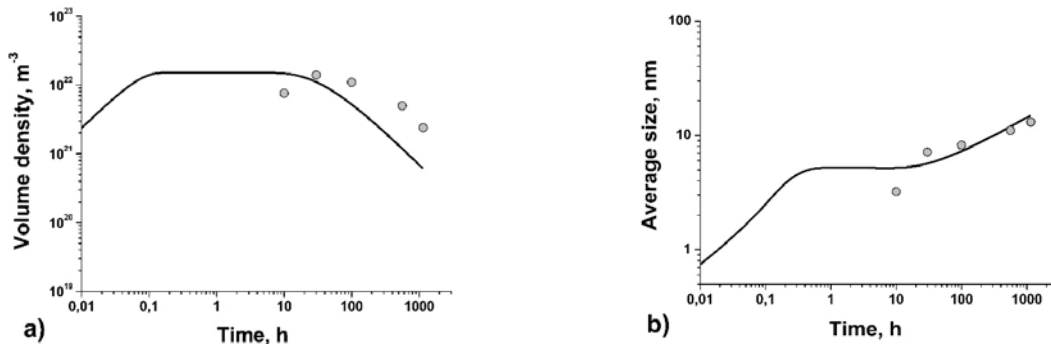


Fig. 6. Model (curves) and experimental (dots, [3]) time dependences of the volume fraction (a) and the average size (b) of V_4C_3 particles in tempering steel B at 600°C

4. Conclusions

The model is developed to predict the kinetics of the recovery and the precipitation of various particles (Fe_3C , V_4C_3 , Mo_2C , Cr_7C_3 , and pure Cu) in Ni-Cr-Mo-V-Cu bainitic-martensitic steels during their cooling after hot rolling and under the subsequent tempering. To evaluate thermodynamic driving forces in the nucleation of the considered particles, equilibrium amounts of SAE (Cr, Mo, V, Cu) dissolved in the ferrite matrix have been calculated using empirical formulas obtained with the Thermo-Calc software. The predicted formation kinetics for the considered carbides and copper particles complies well with relevant experimental data.

Acknowledgments. This work was supported by the grant from the Russian Science Foundation (project No. 19-19-00281).

References

- [1] Rybin VV, Malyshevsky VA, Oleinik VN, Sosenushkin EM, Shorokhova LG. Structural transformations during secondary hardening of low-carbon alloyed steels. *Metal Physics and Metallography*. 1976;41(4): 796-804. (In Russian)
- [2] Yamasaki S, Bhadeshia HKDH. Modelling and characterization of V_4C_3 precipitation and cementite dissolution during tempering of Fe-C-V martensitic steel. *Materials Science and Technology*. 2003;19: 1335-1343.
- [3] Yamasaki S. *Modelling Precipitation of Carbides in Martensitic Steels*. University of Cambridge, PhD Thesis, 2004.
- [4] Pacyna J. The kinetics of phase transformations during tempering in high-speed steels. *Journal of Achievements in Materials and Manufacturing Engineering*. 2007;23(2): 15-18.
- [5] Pacyna J. Dilatometric investigations of phase transformations at heating and cooling of hardened, unalloyed, high-carbon steels. *Journal of Achievements in Materials and Manufacturing Engineering*. 2011;46(1): 7-17.
- [6] Ustinovshchikov YuI, Kovensky IM, Vlasov VA. Mechanism of formation of special carbides in steels alloyed with chromium, molybdenum or vanadium. *Metal Physics and Metallography*. 1976;41(1): 99-111. (In Russian)
- [7] Charleux M, Livet F, Bley F, Louchet F, Brechet Y. Thermal ageing of an Fe-Cu alloy: microstructural evolution and precipitation hardening. *Philosophical Magazine A*. 1996;73: 883-897.
- [8] Deschamps A, Militzer M, Poole WJ. Precipitation kinetics and strengthening of a Fe-0.8wt%Cu alloy. *Iron and Steel Institute of Japan International*. 2001;41(2): 196-205.
- [9] Christien F, Barbu A. Modelling of copper precipitation in iron during thermal aging and irradiation. *Journal of Nuclear Materials*. 2004;324: 90-96.
- [10] Ghosh A, Chatterjee S. Characterization of precipitates in an ultra low carbon Cu bearing high strength steel: A TEM study. *Materials Characterization*. 2005;55: 298-306.
- [11] Fine ME, Isheim D. Origin of copper precipitation strengthening in steel revisited. *Scripta Materialia*. 2005;53: 115-118.
- [12] Soisson F, Fu C-C. Cu-precipitation kinetics in α -Fe from atomistic simulations: Vacancy-trapping effects and Cu-cluster mobility. *Physical Review B*. 2007;76: 1-12.
- [13] Urtsev VN, Mirzaev DA, Yakovleva IL, Vinogradova NI. Transformation of austenite in Fe-Cu alloy. III. Features of copper precipitation during cooling and aging of copper alloyed steels. *Metal Physics and Metallography*. 2008;105(5): 509-515. (In Russian)
- [14] Vasilyev AA, Sokolov DF, Sokolov SF, Kolbasnikov NG. Integral computer model for simulating microstructure evolution during thermomechanical processing and heat treatment of steels and predicting their final mechanical properties. *Materials Science Forum*. 2021;1016: 1532-1537.

- [15] Vasilyev AA, Sokolov DF, Sokolov SF. Modeling microstructure evolution during thermomechanical processing and heat treatment of steels and predicting their mechanical properties. *Materials Physics and Mechanics*. 2020;45(1): 8-19.
- [16] Wagner R, Kampmann R, Voorhees PW. *Homogeneous second-phase precipitation*. In: Kostorz G. (ed.) *Phase transformations in materials*. Weinheim: WILEY-VCH Verlag GmbH; 2001: 309-407.
- [17] Perez M, Dumont N, Acevedo-Reyes D. Implementation of classical nucleation and growth theories for precipitation. *Acta Materialia*. 2008;56: 2119-2132.
- [18] Verdier M, Brechet Y, Guyot P. Recovery of AlMg alloys: flow stress and strain-hardening properties. *Acta Materialia*. 1999;47(1): 127-134.
- [19] Vasilyev AA, Sokolov SF, Golubkov NA, Zisman AA, Sokolov DF, Rudskoy AI. Artifacts of stress relaxation technique to fit recovery activation parameters for low carbon steels. *Materials Physics and Mechanics*. 2019;42: 183-190.
- [20] Frost J, Ashby MF. *Deformation-Mechanism Maps*. Oxford: Pergamon Press; 1982.
- [21] Xu K, Brian G, O'Malley R. Equilibrium model of precipitation in microalloyed steels. *Metallurgical and Materials Transactions A*. 2011;42: 524-539.
- [22] Perez M, Deschamps A. Microscopic modelling of simultaneous two-phase precipitation: application to carbide precipitation in low-carbon steels. *Materials Science and Engineering A*. 2003;360: 214-219.
- [23] Thermo-Calc Software: <http://www.thermocalc.com>
- [24] Vasilyev AA, Golikov PA. *Models for Calculating Carbon Diffusion Coefficient in Steels and Examples of their Practical Use*. St. Petersburg, Peter the Great St. Petersburg Polytechnic University: POLYTECH-PRESS; 2019. (In Russian)
- [25] Bowen A, Leak G. Solute diffusion in alpha- and gamma iron. *Metallurgical Transactions*. 1970;1: 1695-1700.
- [26] Anand MS, Agarwala RP. Diffusion of copper in iron. *Journal of Applied Physics*. 1966;37: 4248-4251.
- [27] Golikov VM, Lazarev VA. Diffusion of copper in iron and Fe-Mo alloys. *Physics and Chemistry of Materials Processing*. 1969;1: 156-159. (In Russian)
- [28] Ghosh A, Mishra B, Das S, Chatterjee S. An ultra low carbon Cu bearing steel: influence of thermomechanical processing and aging heat treatment on structure and properties. *Materials Science and Engineering A*. 2004;374: 43-55.
- [29] Barashev AV, Golubov SI, Bacon DJ, Flewitt PEJ, Lewis TA. Copper precipitation in Fe-Cu alloys under electron and neutron irradiation. *Acta Materialia*. 2004;52: 877-886.